Quaternary Geochronology 49 (2019) 123–130

Contents lists available at ScienceDirect

Quaternary Geochronology

journal homepage: www.elsevier.com/locate/quageo

Luminescence dating of a fluvial sequence using different grain size fractions and implications on Holocene flooding activities in Weihe Basin, central China

Zhong He[a,b,d], Hao Long[b,*], Linhai Yang[c], Jie Zhou[a]

[a] Institute of Soil and Water Conservation, Chinese Academy of Sciences, Ministry of Water Resources, Yangling, 712100, China
[b] State Key Laboratory of Lake Science and Environment, Nanjing Institute of Geography and Limnology, Chinese Academy of Sciences (NIGLAS), Nanjing, 210008, China
[c] Key Laboratory of Desert and Desertification, Northwest Institute of Eco-environment and Resources, Chinese Academy of Sciences, Lanzhou, 730000, China
[d] Institute of Soil and Water Conservation, Northwest A&F University, Yangling, 712100, China

ARTICLE INFO

Keywords:
OSL dating
Fluvial sequence
Flooding activities
Weihe Basin
Chinese Loess Plateau

ABSTRACT

Palaeoflood reconstruction is of great importance to extend the flooding records and improve the understanding of their relationships with climatic change and geomorphologic evolution. As a large active rift basin in central China, Weihe Basin subsided and infilled in response to the uplift of the Tibetan Plateau and Asian monsoon variations. Many rivers drain out the erodible Chinese Loess Plateau with tremendous detritus and then build up considerable fluvial sequences. Scarcity of organic material and potential poor bleaching make the fluvial deposits difficult to date with radiocarbon and optically stimulated luminescence (OSL) technique, and as a result hinder the palaeoflood reconstruction. This study attempts to compare OSL ages resulted from different grain size fractions of quartz, and then cross-checks with independent radiocarbon ages, aiming to choose proper method to reconstruct the chronology of a fluvial sequence from the valley bank of Shichuan River, a tributary of Weihe River. The results show that the coarse quartz grains experienced better bleaching than fine quartz grains, and the comparison with AMS ^{14}C ages further confirms the efficient bleaching of the coarse quartz grains before burial. The sufficient bleaching of the coarse fraction could be attributed to sediment source from the upstream mountainous areas and long-distance transportation. Finally, five palaeoflood events were identified at the times of approximately 2.3–2.6 ka, 3.7–3.9 ka, 4.1–4.7 ka, 6.2–6.8 ka, and 8.9–9.2 ka, corresponding to the periods with intensified rainstorm and vegetation degradation associated with climatic deterioration. This study provides a regional evidence to improve our understanding of the response of river system evolution to climate change.

1. Introduction

Palaeoflood reconstruction plays a key role in extending the flooding records beyond the period covered by gauging-station, and could help us to mitigate flood hazards and improve hydraulic engineering measures in the future (Baker, 1987; Huang et al., 2007; Jones et al., 2012; Thorndycraft et al., 2005). The reconstruction of a complete flood catalog also provides clues for regional palaeohydrology, geomorphology, paleoclimate, soil erosion and their response to atmospheric circulation patterns and global climatic change at a long time scale (Baker, 2008; Benito et al., 2015; Huang et al., 2011; Knox, 2000).

The magnitude and frequency of palaeoflood activities have been reconstructed using the imprint of the flooding on the landscape, including the flood-related channel geomorphology and slackwater deposits (Benito et al., 2015; Guo et al., 2017; Huang et al., 2007, 2011, 2012; Liu et al., 2015; Zhang et al., 2015; Zhou et al., 2016). However, these sedimentary records along a river channel are always sporadically distributed and prone to subsequent erosion (Benito et al., 2003; Yang et al., 2000). Thus, multiple site-based research is still needed to construct a complete flooding catalog and to improve our understanding of the regional response of floods to climate variability.

As a large active rift basin in central China, Weihe Basin subsided and infilled in response to the uplift of the Tibetan Plateau and Asian monsoon variations (Lin et al., 2015; Sun, 2005). Many rivers drain out the erodible Chinese Loess Plateau with tremendous detritus and then build up a considerable fluvial strata interbedded with aeolian loess and palaeosol, which have been extensively used to investigate flood

* Corresponding author.
E-mail addresses: longhao@niglas.ac.cn, lzugeolh@gmail.com (H. Long).

https://doi.org/10.1016/j.quageo.2018.05.007
Received 28 November 2017; Received in revised form 14 April 2018; Accepted 9 May 2018
Available online 10 May 2018
1871-1014/

activities, soil erosion, and associated tectonic and climatic history (Huang et al., 2009, 2011, 2012; Rits et al., 2017; Yang et al., 2000; Zhang et al., 2015).

Considering that radiocarbon dating often suffers from the scarcity of organic material and its vulnerability to contamination by older reworked carbon or younger carbon from plant roots (Long et al., 2011, 2015), optically stimulated luminescence (OSL) dating methods have been more and more applied for age constraints of the relevant fluvial sediment (Guo et al., 2017; Huang et al., 2012; Zhang et al., 2015; Zhao et al., 2016; Zhou et al., 2016). Either fine-grained (FG, 4–11 μm) or coarse-grained (CG, 63–125 μm) fraction has previously been used for dating fluvial sediment. However, more recent studies on modern and imbedded fluvial sediment from the Yellow River found that the FG quartz overestimated the ages significantly compared with the CG quartz counterpart; the reason was attributed to that the CG fraction is mainly derived from the well bleached surface material, while the FG fraction is mainly from the newly eroded loess-palaeosol stratigraphy and poorly bleached prior to deposition (Hu et al., 2010; Zhang et al., 2010). Thus, we also try to compare quartz ages derived from different grain size fractions of the sediment samples from a fluvial sequence in the lower reaches of the Shichuan River, and examine with independent radiocarbon dating, aiming to choose the proper fraction to build up the chronology for the investigated fluvial sequence. Combining with stratigraphic and lithological proxies analysis, the Holocene flooding history and their responses to monsoonal climatic change will be inferred.

2. Geographical settings and sampling

The Weihe Basin is a tectonic depression, which has been caused by its southern and northern boundary faults as well as several inter-faults within the basin (Lin et al., 2015). It is climatically dominated by the East Asia monsoon; the southeast summer monsoon brings a large amount of precipitation, while the dry northwest winter monsoon brings huge aeolian dust to form thick loess sequence. The mean annual temperature and precipitation were ~9.7 °C and ~556 mm, calculated by the data for the last 50 years (National Meteorological Information Center, China, http://data.cma.cn/). In general, the depressed basin is filled with thousands of meters of Cenozoic sediments, over which tens of meters loess is mantling; sedimentary alternation of loess and fluvial deposits can also be seen along rivers or over the alluvial fan.

The Shichuan River, with a total length of about 137 km, a drainage area of 4478 km^2, and annual runoff of 0.215×10^9 m^3, origins from the Beishan mountains (1400–1800 m a.s.l.), flows through the loess tablelands (500–1000 m a.s.l.) and into the Weihe River in the low-lying alluvial plains (350–450 m a.s.l.) (Fig. 1a and b). A 12 m depth outcrop (named by YC as nearby Yao-Cun village), composed of interbeded loess, palaeosol and slackwater deposit (SWD), was exposed by a brickyard soil-taken field on the lowerest terrace of the Shichuan River (Fig. 1c and d). The loess layer is characterized by yellowish fine-medium silt without sedimentary structures; the palaeosol layer mainly consists of dark brown clayey silt with relatively more organic matter; while the SWD layer is dominated by two units, i.e., a coarse silty sand layer with parallel and waving bedding and an overlying thin clayey silt layer (Fig. 1). Five SWD layers were identified according to close examination of the color, texture and structure in the YC profile during field investigation. A total of 14 OSL samples were taken with steel cylinder from the profile (at the interval of 80–100 cm) (Fig. 1), and immediately packed with light-proof bags during the fieldwork, while bulk samples for proxies measurement were collected at 2 cm interval.

3. Laboratory analysis methods

3.1. Luminescence dating

Samples were first treated with 30% H_2O_2 and 10% HCl to remove organic matter and carbonates respectively, and followed by wet sieving. The CG quartz fraction was separated with heavy liquid (sodium polytungstate, 2.62–2.70 g/cm^3) and then etched with 40% HF for 40 min to dissolve feldspars and the alpha-irradiated layer (~20 μm). The FG quartz fraction was separated according to Stokes' law and etched with 30% H_2SiF_6 (fluorosilicic acid) for 5–7 days at room temperature to dissolve feldspars. Then both fractions were rinsed with 10% HCl to remove fluoride precipitates. We obtained sufficient CG quartz only from eight of 14 samples, as other six samples are dominated by FG sediment. The purity of the isolated quartz was checked using the infrared (IR) depletion ratio (Duller, 2003), and no obvious infrared stimulated luminescence (IRSL) signals were observed in any sample.

All luminescence measurements were carried out in the NIGLAS Luminescence Dating Laboratory with an automated luminescence reader (Risø TL/OSL DA-20) equipped with stimulation units of blue LEDs (470 nm) and infrared light (~870 nm), and a $^{90}Sr/^{90}Y$ beta source. The quartz OSL signal was detected by a 9235QA photomultiplier tube through a 7.5 mm thick U-340 filter. D_e value of quartz was determined using a single-aliquot regenerative-dose (SAR) protocol (Murray and Wintle, 2000).

The concentration of radioactive nuclides (U, Th and K) was measured by neutron activation analysis at the China Institute of Atomic Energy (Beijing). The cosmic ray dose rate was estimated as a function of depth, altitude, and geomagnetic latitude according to Prescott and Hutton (1994). The total dose rates were finally calculated using the conversion factors of Guérin et al. (2011).

3.2. Radiocarbon dating

Radiocarbon dating was carried out at the Beta Analytic Inc. The samples were processed using a conventional acid–alkali–acid treatment to remove carbonates and other contaminants and then prepared as graphite for AMS radiocarbon measurements (Mook and Streurman, 1983). The AMS ^{14}C ages were calibrated to calendar years using the CALIB program with the IntCal13 dataset after $^{13}C/^{12}C$ adjustment (Reimer et al., 2013), which allows direct comparison with OSL ages (Table S1).

3.3. Proxy measurements

Considering significant changes in magnetic susceptibility (MS) and particle-size distribution in different sedimentary environments (Fig. 1), these proxies can be used for the identification of stratigraphic subdivision and SWDs, combined with field observation on the lithology and stratigraphy. MS was measured on a mass of 10 g of dry ground sediment using a Bartington MS-2 magnetic susceptibility meter at both low (0.47 kHz) and high (4.7 kHz) frequencies. Particle-size distribution of the samples was analyzed using a Malvern Mastersizer-2000 laser analyzer (with a measurement range of 0.02–2000 μm) with $(NaPO_3)_6$ as a dispersing agent after pretreatment with 10% HCl and 10% H_2O_2 for eliminating the organic matter and carbonates, respectively.

4. Results and discussions

4.1. Identification of palaeoflood events

The YC profile is generally composed of interbeded SWDs, loess, and palaeosol. The stratigraphic subdivisions were determined firstly based on a close field observation on the color, texture and structure of sediments from the profile (Fig. 1). The upper four SWD layers mainly consist of coarse silty sand with obvious parallel and waving bedding capped by a thin clayey silt layer; the lowermost SWD consists of at least 10 sedimentary alternations of dull yellow orange sandy silt and pale brown silty clay. The MS of SWDs is much smaller (Fig. 1d), and its

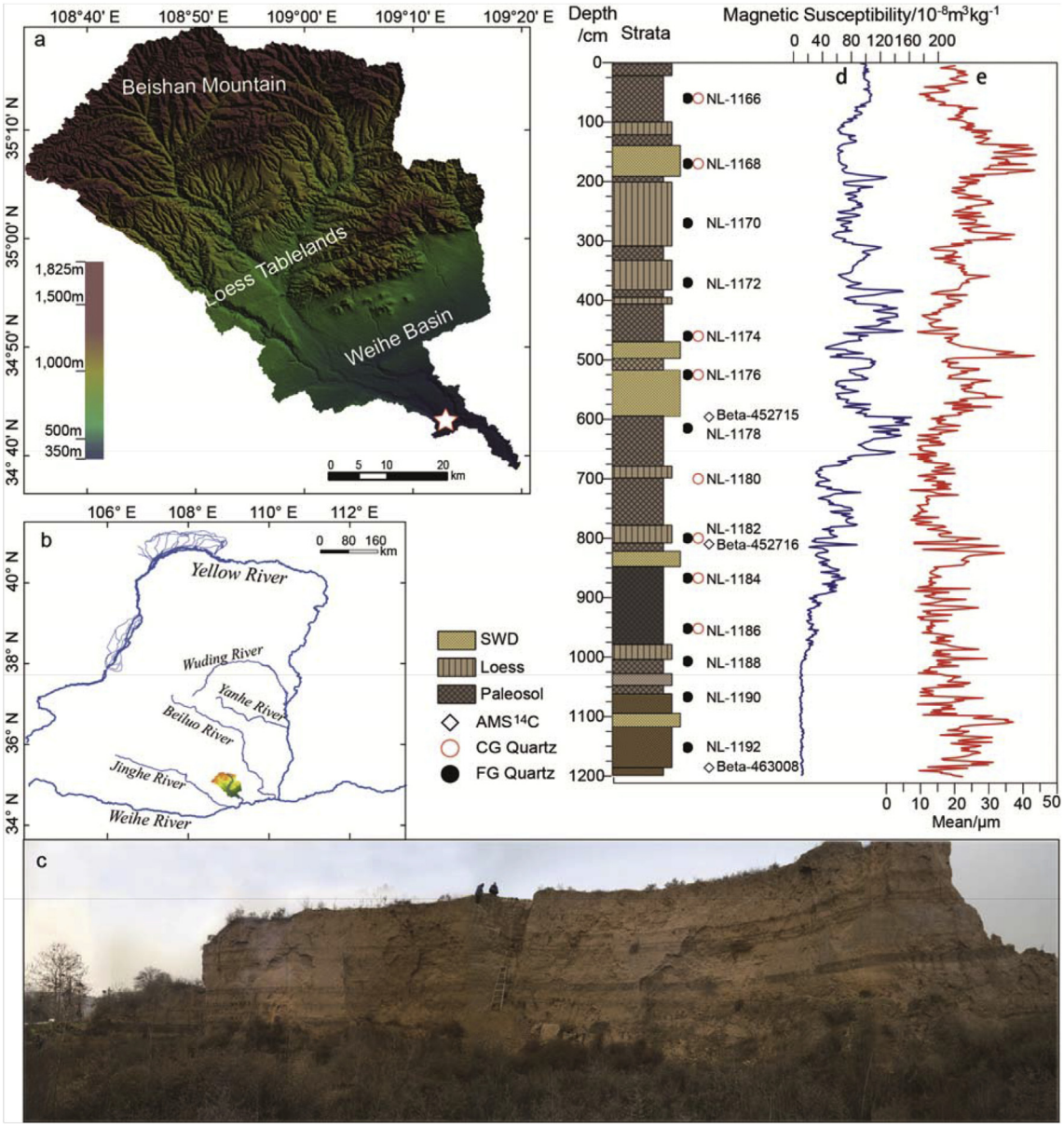

Fig. 1. (a) Topographic map of Shichuan River drainage (white pentagram shows the location of YC profile); (b) location of the Shichuan River in the Yellow river watershed; (c) panoramic photo of the YC profile; stratigraphy subdivision and OSL-samples location, and the analysis results of magnetic susceptibility (d) and mean grain size (e). (For interpretation of the references to color in this figure legend, the reader is referred to the Web version of this article.)

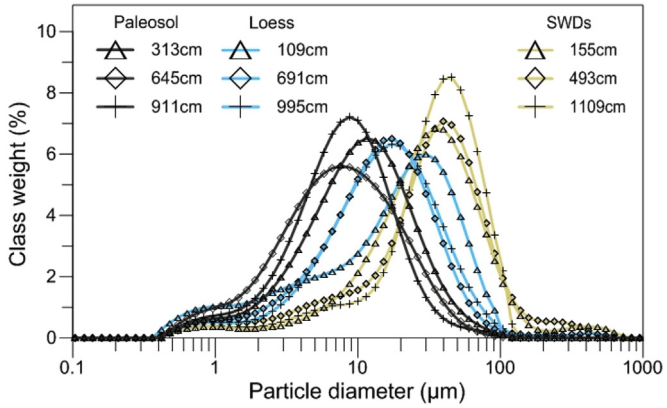

Fig. 2. Particle size distribution of representative samples at different depth.

mean grain size is much coarser (Fig. 1e) compared with underlying and overlying loess and palaeosol as well as the loess from the surrounding sites (Kang et al., 2013; Yang and Ding, 2017); similar observations on the SWD have been reported by previous studies (Guo et al., 2017; Huang et al., 2011, 2012). Furthermore, the particle-size distribution of these SWDs appears to be rather distinguishable from those of the aeolian loess and soil layer (Fig. 2). The distinct characteristics of MS and grain size further support the identification of five SWD layers in the investigated profile.

4.2. OSL characteristics, ages and comparison with radiocarbon dates

In order to select a proper thermal treatment, preheat plateau tests were conducted on both CG and FG quartz fractions of a young sample NL-1166 (Fig. 3a, and Fig. S1a), and also on the FG fraction of an old sample NL-1190 (Fig. S1c). All of these results showed D_e value is rather insensitive to preheat temperatures; recycling ratios are almost within unity, and recuperations are generally lower than 5% for all preheat

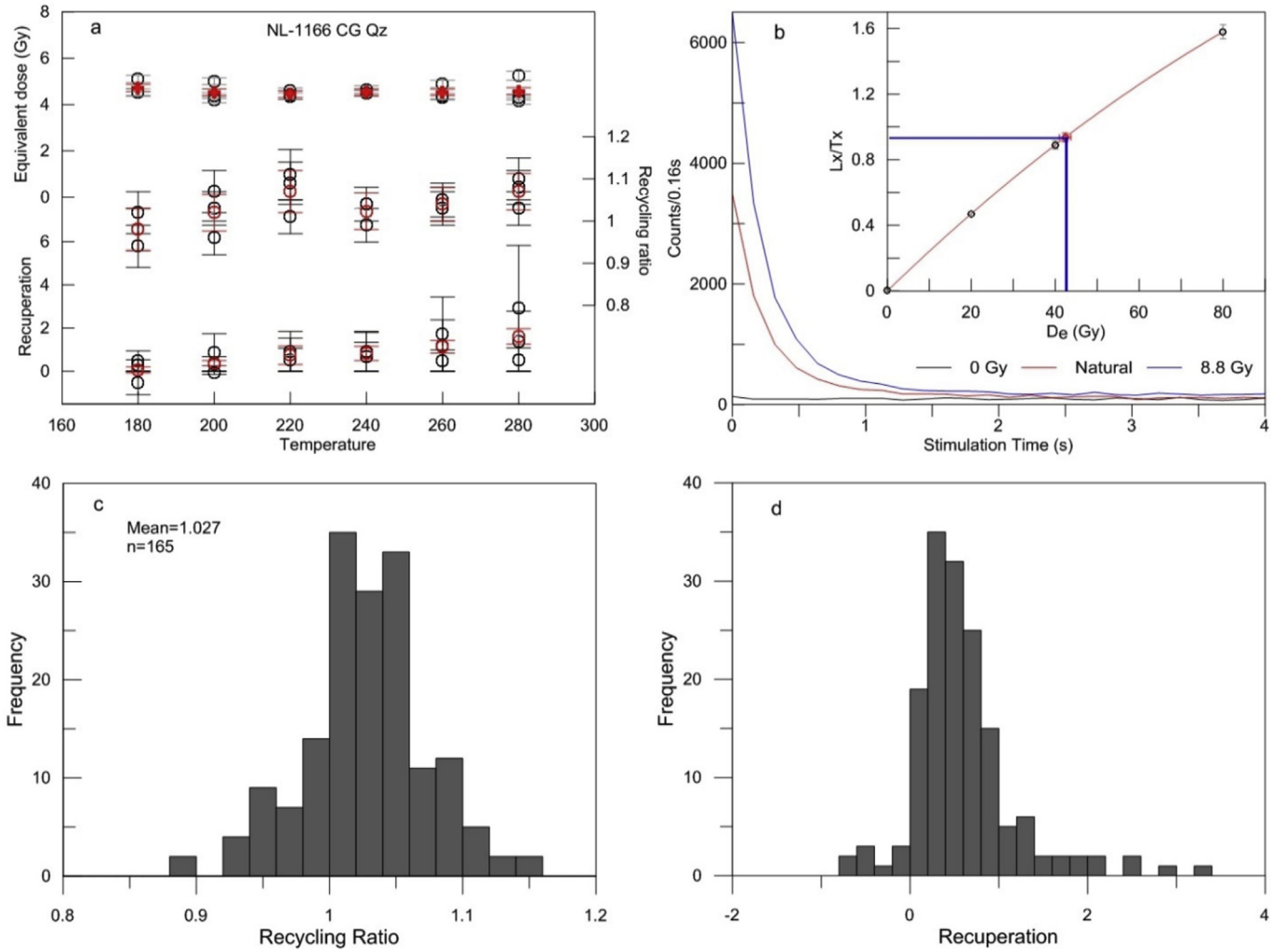

Fig. 3. (a) Preheat plateau test (red circle is the average value of three aliquots and black circle denotes each of three aliquots); (b) growth curve of sample NL-1166 (CG quartz); and histograms summarizing recycling ratios (c) and recuperations (d) for all measured aliquots of CG fraction. (For interpretation of the references to color in this figure legend, the reader is referred to the Web version of this article.)

temperature. In addition, dose recovery tests for various preheat temperatures were carried out on the same two samples. As shown in Figs. S1b and d, there are recovery ratio plateaus below 240 °C. Finally, we chose a preheat temperature of 200 °C for the following measurements.

The decay curves from a representative sample (NL-1166) show that the OSL signals decay to the background within ~1 s (Fig. 3b), indicating that the signals are dominated by the fast component and it can be sufficiently bleached in a very short time. The average recycling ratio of CG and FG quartz is 1.027 (Fig. 3c, n = 165) and 1.042 (Fig. S1e, n = 116), confirming that the sensitivity corrections work well and the measurement following laboratory irradiations is reproducible. The majority of recuperations of both the CG and FG quartz are less than 2%, acceptably small (Fig. 3d and Fig. S1f). The dose distributions of most CG quartz samples are fairly narrow with small overdispersion (OD) values (5.9–15.9%) (Fig. 4). Different age models are very likely to yield similar age results. Thus, we used central age model (CAM) for age calculation (Galbraith et al., 1999), which has the advantage over the weighted mean of including all the available data without discarding outliers (Long and Shen, 2017). The results of equivalent dose, dose rate and OSL age for CG and FG quartz are summarized in Table S2.

Although both the CG and FG quartz seemed to behave well for OSL SAR dating, the chronology results show great differences between CG and FG quartz ages (Table S2 and Fig. 5). The OSL ages derived from CG quartz are generally consistent with the stratigraphic order, but FG quartz ages are severely inverse, and obviously much older than the CG quartz counterpart. In the field, the sample at 596 cm was sieved with a lot of carefulness to separate the charcoals out of bulk sediments. Unfortunately, we still observed small pieces of roots within this charcoal-dominated sample. The younger carbon from root contamination could be the reason for the radiocarbon age underestimation compared with chronological framework based on CG quartz ages. In contrast, bulk organic matter was used for radiocarbon dating of the other two dark layers (810 cm and 1186 cm) because charcoals are too limited to date. The agreement between CG OSL age and radiocarbon dates confirmed the robustness of two kinds of chronologies for this two layers. We thus conclude that the CG quartz fraction is more likely to be sufficiently bleached than FG quartz fraction, and have greater confidence on the CG quartz based chronology for the investigated sequence. The charcoal sample at 596 cm, suffering from younger carbon contamination, was not used for age framework construction.

The discrepancy of bleaching conditions between CG and FG fractions might be caused by different sediment sources, transportation distance and manner. The FG fraction may mostly source from the nearby or upstream clayey loess due to rainstorm and erosion. The partial bleaching of FG fraction is attributed to its aggregate effect during transportation as hyper-concentrated flow. The Shichuan River flows through a clayey loess zone in its middle and lower reaches,

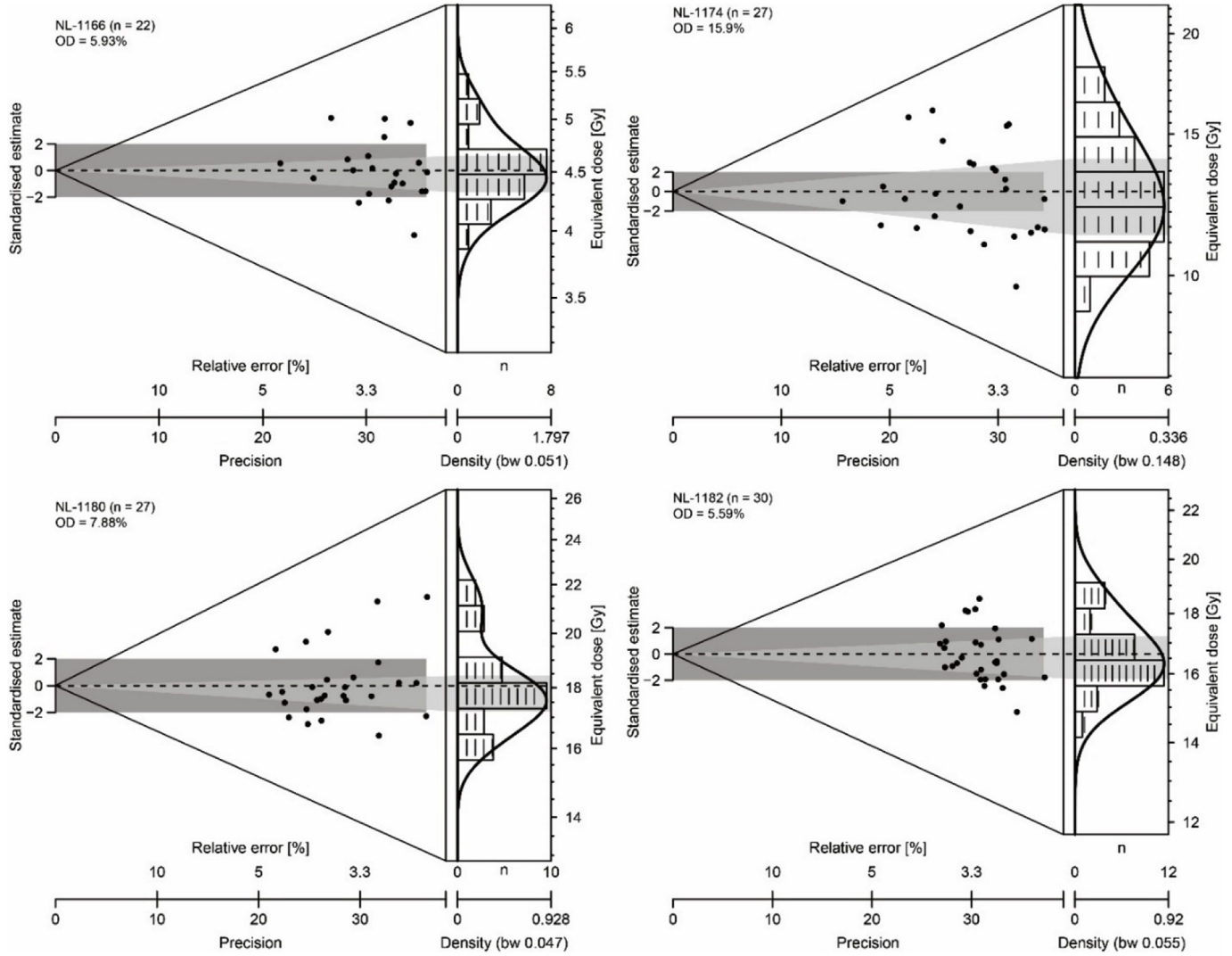

Fig. 4. D_e distributions for representative CG samples.

where the coarse component (> 63 μm) is only about 3–6% of the loess layers and less than 2% of the palaeosol units (Yang and Ding, 2017). In contrast, its headwater originates from mountain areas characterized with weathered bedrock and larger stream gradient, and is very potential to provide huge amount of coarse-grain dominated sand for fluvial sedimentation. Thus, the sandy component (> 63 μm) from the investigated sedimentary sequence could have experienced long-distance transportation, and then sufficient bleaching before deposition. Our results support earlier studies on modern fluvial sand and late Pleistocene hyper-concentrated flow deposit of the Yellow River; they also suggested that the coarse grains were mainly contributed by the well bleached surface material, while the fine grains were mainly from the newly eroded loess-palaeosol strata and thus experienced poorly bleaching (Hu et al., 2010; Zhang et al., 2010). It is noted that the FG quartz ages of loess layer were also overestimated compared with CG based chronology. The reason could be attributed to the nearby source from the floodplain of Shichuan River and the subsequent fast accumulation for loess formation over the river bank, leading to insufficient bleaching; this is different from the typical loess from Chinese Loess Plateau. The high deposition rate of our sedimentary sequence, about five times as high as that of the surrounding Holocene loess sequence, is likely to indicate a great contribution of local source to sediment accumulation. Recent study on Mangshan loess also attributed its high deposition rate to major dust supply from the nearby lower Yellow River floodplain (Shang et al., 2018). Short-distance transportation could give rise to insufficient bleaching and hence age overestimate of FG quartz. Therefore, we recommend that multiple signal comparison could help us to choose proper fraction for OSL dating, especially for the fluvial sequence related to waterlain deposits.

Based on the OSL ages of CG quartz fraction and radiocarbon ages, the chronology of YC fluvial sequence was reconstructed. The age-depth model of the whole sequence (Fig. S2) was retrieved via software Bacon 2.2 using Bayesian statistics (Blaauw and Christen, 2011).

4.3. Regional comparison of palaeoflood events and possible causes

The environment in the Weihe Basin is very sensitive to climatic changes as it lies in semiarid and sub-humid zones, where the precipitation is dominated by the East Asian monsoon. Modern floods in this area often result from abnormal atmospheric circulation that are closely related with intensified climatic variations (Huang et al., 2013). According to our study, five palaeoflood events were identified at approximately 2.3–2.6 ka, 3.7–3.9 ka, 4.1–4.7 ka, 6.2–6.8 ka, and 8.9–9.2 ka, which were also recorded in the Yellow River and other river systems in the East Asian monsoon region. It seems that these palaeoflood events correspond to episodes of strengthened climatic variability and instability which was probably caused by monsoonal shift (Fig. 6). For example, the palaeoflood at 8.9–9.2 ka occurred at the transition from

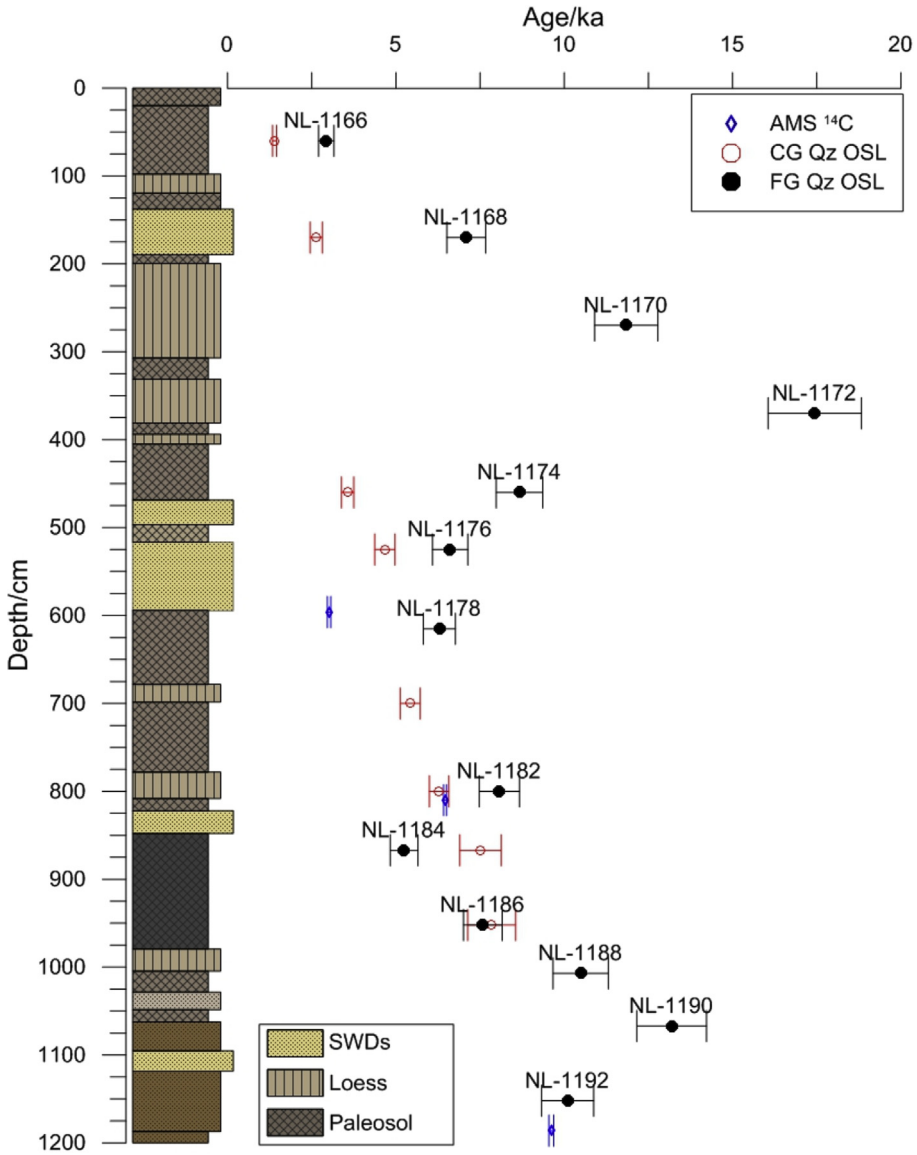

Fig. 5. Comparison of ages based on CG and FG quartz OSL and AMS ^{14}C.

cold-dry early Holocene to humid-wet mid Holocene, with less precipitation and gradually increasing temperature; and this event was also found in the Yanhe River (Guo et al., 2017) and the Sushui River (Huang et al., 2007). The palaeoflood of 6.2–6.8 ka occurred at interval with lower precipitation and decreasing temperature; and it was also recorded in the Hanjiang River (Guo et al., 2015) and middle reaches of the Yellow River (Yang et al., 2000). The palaeofloods at 2.3–2.6 ka, 3.7–3.9 ka, and 4.1–4.7 ka occurred at the transition from mid Holocene Megathermal to cool-dry late Holocene, accompanied with decreasing in global temperature and precipitation as recorded by the lower $\delta^{18}O$ values from stalagmites Dongge cave (Fig. 6c and d). The relative higher number of ENSO events also caused climate instability in the studied area (Fig. 6f). The sediment records of palaeoflood event at 4.1–4.7 ka were also extensively distributed in the Guanting Basin of the upper Yellow River (Ma et al., 2014), the Qishuihe River (Huang et al., 2011), the Beiluohe River (Zhang et al., 2015), the Yihe River (Shen et al., 2015), the Jinghe River (Huang et al., 2012) and the Hanjiang River (Liu et al., 2015). The palaeoflood event at 2.3–2.6 ka was also found in the Guanting Basin (Ma et al., 2014), middle reach of the Yellow River (Huang et al., 2007), the Yongding River (Zhao et al., 2017), the upper and middle Yangtze River (Huang et al., 2013).

The comparison above appears to indicate that these palaeofloods occurred at interval with decreased precipitation. This phenomenon has been reported by previous studies from the upper Hanjiang River and middle Yellow River, where majority of palaeofloods and droughts happened at the same periods (Huang et al., 2011; Liu et al., 2014). The reason why the flood frequency and magnitude were higher during the relative dry periods could be attributed to three aspects. Firstly, vegetation degradation associated with climate deterioration would increase the probability of flood occurrence. Vegetation plays a crucial role in flood control via increasing interception of precipitation, improving the infiltration rate, slowing down or retaining runoff, and increasing evapotranspiration, consequently delaying or even reducing runoff. This has been proved by the sharp decrease of runoff and sediment in the Yellow River after the vegetation restoration in the Chinese Loess Plateau during the past 20 years (Zhao et al., 2014). In the water-limited semi-arid to semi-humid environments, even modest precipitation decline could cause vegetation degradation and soil development cessation. The consistence between the timing of palaeofloods and lower probability density of palaeosol ages in the Chinese Loess Plateau also suggests that floods are prone to occurence at periods with vegetation degradation under climate deterioration (Fig. 6e). Secondly, even

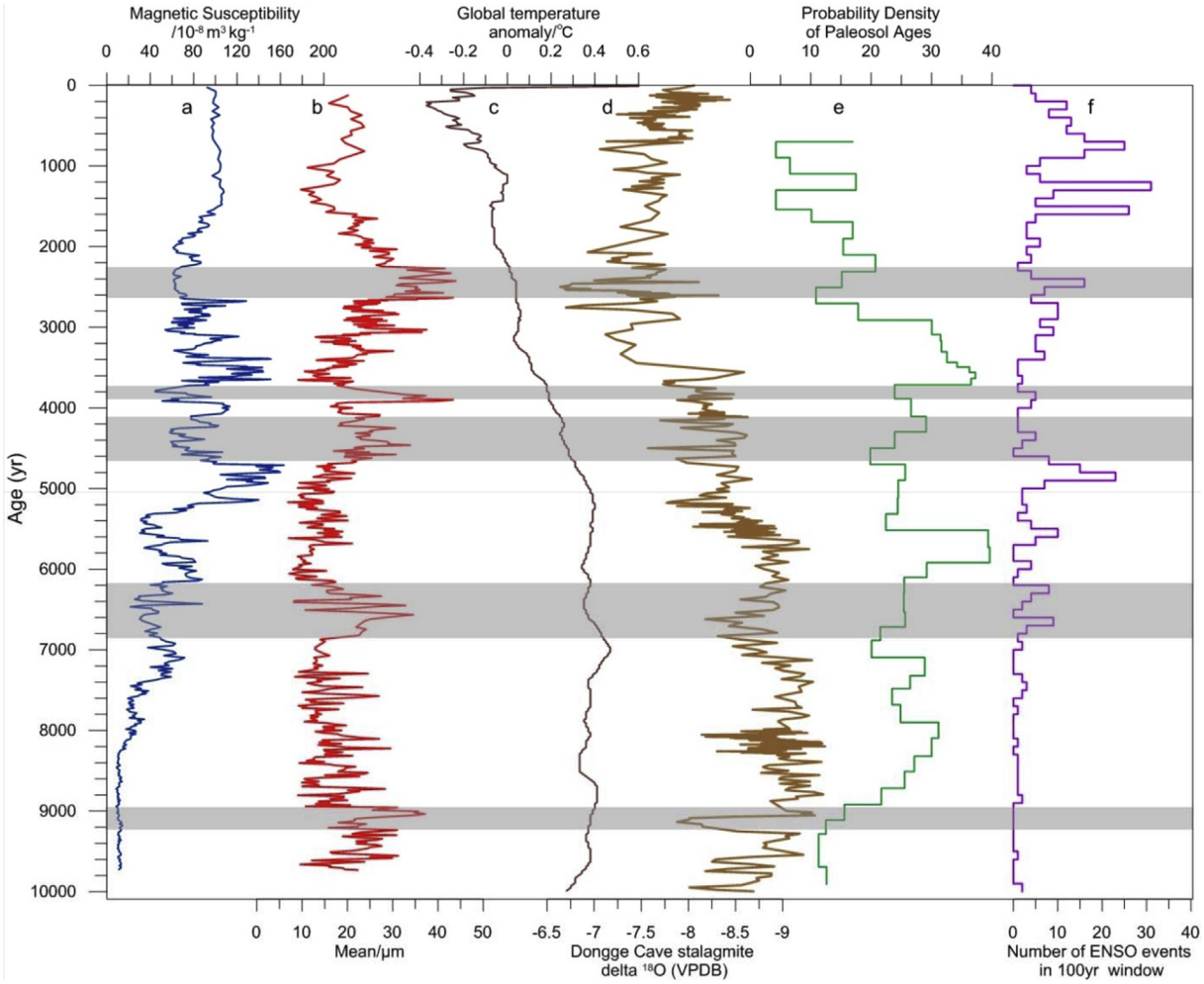

Fig. 6. (a) MS curve of YC profile; (b) mean grain-size sequence for YC profile; (c) global temperature anomaly (Marcott and Mix, 2013); (d) stalagmites $\delta^{18}O$ values from the Dongge cave (Wang et al., 2005); (e) probability density of palaeosol ages in the Chinese Loess Plateau (Wang et al., 2014); (f) number of ENSO events in 100 yr window (Moy et al., 2002); gray bars represent the timing of palaeoflood.

though the mean annual precipitation was reduced, the extreme rainstorm did not necessarily decrease but rather higher amounts and lower frequency (Shen et al., 2015). Without vegetation protection, rainstorm with higher amounts and lower frequency is more likely to cause flooding. Thirdly, the channels were prone to being filled with deposits due to the less river flow and decreased hydrodynamic force during the arid period, which hindered the pass of flood peaks and formed floods and associated disaster (Wang et al., 2017).

5. Conclusions

Based on close visible observation together with proxies' analysis, we identified five palaeoflood sediment units in a fluvial sequence from the lower reaches of the Shichuan River (Weihe Basin). Based on cross-checking with independent radiocarbon ages, comparison of quartz OSL ages between coarse and fine grains suggested that the coarse quartz grains experienced better bleaching than fine grains in the fluvial sediment. Combined the CG quartz OSL ages and radiocarbon dates, timing of these palaeofloods events were constrained at approximately 2.3–2.6 ka, 3.7–3.9 ka, 4.1–4.7 ka, 6.2–6.8 ka, and 8.9–9.2 ka, corresponding to episodes of intensified rainstorm and vegetation degradation, which might have been related to the high frequency of climatic variability and instability forced by monsoonal shift. This study provides regional evidence on the response of a river system to climate changes.

Acknowledgement

This study was supported by grants from the Natural Science Foundation of China (No. 41472156, No. 41472144), the West Light Foundation of the Chinese Academy of Science to Zhong He, and the Youth Innovation Promotion Association CAS (No. 2015251) to Hao Long. We thank the anonymous reviewers for the helpful and constructive suggestions of the manuscript.

Appendix A. Supplementary data

Supplementary data related to this article can be found at http://dx.doi.org/10.1016/j.quageo.2018.05.007.

References

Baker, V.R., 1987. Palaeoflood hydrology and extreme flood events. J. Hydrol. 96, 79–99.
Baker, V.R., 2008. Paleoflood hydrology: origin, progress, prospects. Geomorphology 101, 1–13.
Benito, G., Macklin, M.G., Zielhofer, C., Jones, A.F., Machado, M.J., 2015. Holocene flooding and climate change in the Mediterranean. Catena 130, 13–33.
Benito, G., Sanchez-Moya, Y., Sopena, A., 2003. Sedimentology of high-stage flood deposits of the Tagus River, Central Spain. Sediment. Geol. 157, 107–132.
Blaauw, M., Christen, J.A., 2011. Flexible paleoclimate age-depth models using an autoregressive gamma process. Bayesian Anal. 6, 457–474.
Duller, G.A.T., 2003. Distinguishing quartz and feldspar in single grain luminescence measurements. Radiat. Meas. 37, 161–165.
Galbraith, R.F., Roberts, R.G., Laslett, G.M., Yoshida, H., Olley, J.M., 1999. Optical dating

of single and multiple grains of quartz from Jinmium rock shelter, northern Australia: part I, experimental design and statistical models. Archaeometry 41, 339–364.
Guérin, G., Mercier, N., Adamiec, G., 2011. Dose-rate conversion factors: update. Ancient TL 29, 5–8.
Guo, Y.Q., Huang, C.C., Pang, J.L., Zha, X.C., Zhou, Y.L., Wang, L.S., Zhang, Y.Z., Hu, G.M., 2015. Investigating extreme flood response to Holocene palaeoclimate in the Chinese monsoonal zone: a palaeoflood case study from the Hanjiang River. Geomorphology 238, 187–197.
Guo, Y.Q., Huang, C.C., Pang, J.L., Zhou, Y.L., Zha, X.C., Mao, P.N., 2017. Reconstruction palaeoflood hydrology using slackwater flow depth method in the Yanhe River valley, middle Yellow River basin, China. J. Hydrol. 544, 156–171.
Hu, G., Zhang, J.F., Qiu, W.L., Zhou, L.P., 2010. Residual OSL signals in modern fluvial sediments from the Yellow River (HuangHe) and the implications for dating young sediments. Quat. Geochronol. 5, 187–193.
Huang, C.C., Pang, J., Zha, X., Zhou, Y., Yin, S., Su, H., Zhou, L., Yang, J., 2013. Extraordinary hydro-climatic events during the period AD 200 − 300 recorded by slackwater deposits in the upper Hanjiang River valley, China. Palaeogeogr. Palaeoclimatol. Palaeoecol. 374, 274–283.
Huang, C.C., Pang, J.L., Su, H.X., Li, S.L., Ge, B.W., 2009. Holocene environmental change inferred from the loess-palaeosol sequences adjacent to the floodplain of the Yellow River, China. Quat. Sci. Rev. 28, 2633–2646.
Huang, C.C., Pang, J.L., Zha, X.C., Su, H.X., Jia, Y.F., 2011. Extraordinary floods related to the climatic event at 4200 a BP on the Qishuihe River, middle reaches of the Yellow River, China. Quat. Sci. Rev. 30, 460–468.
Huang, C.C., Pang, J.L., Zha, X.C., Su, H.X., Jia, Y.F., Zhu, Y.Z., 2007. Impact of monsoonal climatic change on Holocene overbank flooding along Sushui River, middle reach of the Yellow River, China. Quat. Sci. Rev. 26, 2247–2264.
Huang, C.C., Pang, J.L., Zha, X.C., Zhou, Y.L., Su, H.X., Zhang, Y.Z., Wang, H.S., Gu, H.L., 2012. Holocene palaeoflood events recorded by slackwater deposits along the lower Jinghe River valley, middle Yellow River basin, China. J. Quat. Sci. 27, 485–493.
Jones, A.F., Macklin, M.G., Brewer, P.A., 2012. A geochemical record of flooding on the upper River Severn, UK, during the last 3750 years. Geomorphology 179, 89–105.
Kang, S., Wang, X., Lu, Y., 2013. Quartz OSL chronology and dust accumulation rate changes since the Last Glacial at Weinan on the southeastern Chinese Loess Plateau. Boreas 42, 815–829.
Knox, J.C., 2000. Sensitivity of modern and Holocene floods to climate change. Quat. Sci. Rev. 19, 439–457.
Lin, A., Rao, G., Yan, B., 2015. Flexural fold structures and active faults in the northern–western Weihe Graben, central China. J. Asian Earth Sci. 114, 226–241.
Liu, T., Huang, C.C., Pang, J., Zhou, Y., Zhang, Y., Ji, L., Shang, R., 2014. Extraordinary hydro-climatic events during 1800–1600yr BP in the Jin–Shaan Gorges along the middle Yellow river, China. Palaeogeogr. Palaeoclimatol. Palaeoecol. 410, 143–152.
Liu, T., Huang, C.C., Pang, J.L., Zha, X.C., Zhou, Y.L., Zhang, Y.Z., Ji, L., 2015. Late Pleistocene and Holocene palaeoflood events recorded by slackwater deposits in the upper Hanjiang River valley, China. J. Hydrol. 529, 499–510.
Long, H., Lai, Z., Wang, N., zhang, J., 2011. A combined luminescence and radiocarbon dating study of Holocene lacustrine sediments from arid northern China. Quat. Geochronol. 6, 1–9.
Long, H., Shen, J., 2017. Sandy beach ridges from Xingkai lake (NE Asia): timing and response to palaeoclimate. Quat. Int. 430, 21–31.
Long, H., Shen, J., Wang, Y., Gao, L., Frechen, M., 2015. High-resolution OSL dating of a late Quaternary sequence from Xingkai lake (NE Asia): chronological challenge of the “MIS 3a Mega-paleolake” hypothesis in China. Earth Planet Sci. Lett. 428, 281–292.
Ma, M.M., Dong, G.H., Chen, F.H., Meng, X.M., Wang, Z.L., Elston, R., Li, G.Q., 2014. Process of paleofloods in Guanting basin, Qinghai Province, China and possible relation to monsoon strength during the mid-Holocene. Quat. Int. 321, 88–96.
Marcott, S.A., Mix, A.C., 2013. A reconstruction of regional and global temperature for the past 11,300 years. Science 339, 1198.
Mook, W.G., Streurman, H.J., 1983. Physical and chemical aspects of radiocarbon dating. In: Proceedings of the First International Symposium C & Archaeology Groningen, vol. 8. pp. 31–55.
Moy, C.M., Seltzer, G.O., Rodbell, D.T., Anderson, D.M., 2002. Variability of El Nino/ southern oscillation activity at millennial timescales during the Holocene epoch. Nature 420, 162–165.
Murray, A.S., Wintle, A.G., 2000. Luminescence dating of quartz using an improved single-aliquot regenerative-dose protocol. Radiat. Meas. 32, 57–73.
Prescott, J.R., Hutton, J.T., 1994. Cosmic ray contribution to dose rates for luminescence and ESR dating: large depths and long-term time variations. Radiat. Meas. 23, 497–500.
Reimer, P.J., Bard, E., Bayliss, A., Beck, J.W., Blackwell, P.G., Bronk Ramsey, C., Buck, C.E., Cheng, H., Edwards, R.L., Friedrich, M., 2013. IntCal13 and Marine 13 radiocarbon age calibration curves 0-50,000 Years cal BP. Radiocarbon 55, 1869–1887.
Rits, D.S., van Balen, R.T., Prins, M.A., Zheng, H., 2017. Evolution of the alluvial fans of the Luo River in the Weihe Basin, central China, controlled by faulting and climate change - a reevaluation of the paleogeographical setting of Dali Man site. Quat. Sci. Rev. 166, 339–351.
Shang, Y., Prins, M.A., Beets, C.J., Kaakinen, A., Lahaye, Y., Dijkstra, N., Rits, D.e.S., Wang, B., Zheng, H., Balen, R.T.v., 2018. Aeolian dust supply from the Yellow River floodplain to the Pleistocene loess deposits of the Mangshan Plateau, central China_ Evidence from zircon U-Pb age spectra. Quat. Sci. Rev. 182, 131–143.
Shen, H.Y., Yu, L.P., Zhang, H.M., Zhao, M., Lai, Z.P., 2015. OSL and radiocarbon dating of flood deposits and its paleoclimatic and archaeological implications in the Yihe River Basin, East China. Quat. Geochronol. 30, 398–404.
Sun, J., 2005. Long-term fluvial archives in the Fen Wei Graben, central China, and their bearing on the tectonic history of the India?Asia collision system during the Quaternary. Quat. Sci. Rev. 24, 1279–1286.
Thorndycraft, V.R., Benito, G., Rico, M., Sopena, A., Sanchez-Moya, Y., Casas, A., 2005. A long-term flood discharge record derived from slackwater flood deposits of the Llobregat River, NE Spain. J. Hydrol. 313, 16–31.
Wang, H., Wu, X., Bi, N., Li, S., Yuan, P., Wang, A., Syvitski, J.P.M., Saito, Y., Yang, Z., Liu, S., Nittrouer, J., 2017. Impacts of the dam-orientated water-sediment regulation scheme on the lower reaches and delta of the Yellow River (Huanghe): a review. Global Planet. Change 157, 93–113.
Wang, H.P., Chen, J.H., Zhang, X.J., Chen, F.H., 2014. Palaeosol development in the Chinese Loess Plateau as an indicator of the strength of the East Asian summer monsoon: evidence for a mid-Holocene maximum. Quat. Int. 334, 155–164.
Wang, Y., Cheng, H., Edwards, R.L., He, Y., Kong, X., An, Z., Wu, J., Kelly, M.J., Dykoski, C.A., Li, X., 2005. The Holocene Asian monsoon: links to solar changes and North Atlantic climate. Science 308, 854–857.
Yang, D.Y., Yu, G., Xie, Y.B., Zhan, D.J., Li, Z.J., 2000. Sedimentary records of large Holocene floods from the middle reaches of the Yellow River, China. Geomorphology 33, 73–88.
Yang, S.L., Ding, Z.L., 2017. Spatial changes in grain size of loess deposits in the Chinese Loess Plateau and implications for palaeoenvironment. Quat. Sci. 37, 934–944.
Zhang, J.F., Qiu, W.L., Wang, X.Q., Hu, G., Li, R.Q., Zhou, L.P., 2010. Optical dating of a hyperconcentrated flow deposit on a Yellow River terrace in Hukou, Shaanxi, China. Quat. Geochronol. 5, 194–199.
Zhang, Y.Z., Huang, C.C., Pang, J.L., Zha, X.C., Zhou, Y.L., Wang, X.Q., 2015. Holocene palaeoflood events recorded by slackwater deposits along the middle Beiluohe River valley, middle Yellow River basin, China. Boreas 44, 127–138.
Zhao, G., Tian, P., Mu, X., Jiao, J., Wang, F., Gao, P., 2014. Quantifying the impact of climate variability and human activities on streamflow in the middle reaches of the Yellow River basin, China. J. Hydrol. 519, 387–398.
Zhao, X.H., Wang, J.P., Wei, M.J., Lai, Z.P., Fan, M.J., Zhao, J.X., Pan, B.L., Zhao, Y.H., Li, X.P., Zhao, Q.Y., 2017. Optically stimulated luminescence dating of Holocene palaeoflood deposits in the middle reach of the Yongding River, China. Quat. Int. 453, 37–47.
Zhao, X.R., Huang, C.C., Pang, J.L., Zha, X.C., Guo, Y.Q., Hu, G.M., 2016. Holocene climatic events recorded in palaeoflood slackwater deposits along the middle Yiluohe River valley, middle Yellow River basin, China. J. Asian Earth Sci. 123, 85–94.
Zhou, L., Huang, C.C., Zhou, Y.L., Pang, J.L., Zha, X.C., Xu, J., Zhang, Y.Z., Guo, Y.Q., 2016. Late Pleistocene and Holocene extreme hydrological event records from slackwater flood deposits of the Ankang east reach in the upper Hanjiang River valley, China. Boreas 45, 673–687.